The protein and neutral lipid composition of lipid droplets isolated from the fission yeast, *Schizosaccharomyces pombe*

Alex Meyers[1], Karuna Chourey[2], Taylor M. Weiskittel[1], Susan Pfiffner[3], John R. Dunlap[3,4], Robert L. Hettich[2], and Paul Dalhaimer[1,3,5]*

1Department of Chemical and Biomolecular Engineering, University of Tennessee, Knoxville, TN 37996-2200, USA
2Oak Ridge National Laboratory, Oak Ridge, TN 37831, USA
3Department of Biochemistry, Cellular and Molecular Biology, University of Tennessee, Knoxville, TN 37996, USA
4Advanced Microscopy and Imaging Center, University of Tennessee, Knoxville, TN 37996, USA
5Institute of Biomedical Engineering, University of Tennessee, Knoxville, TN 37996, USA

Abstract: Lipid droplets consist of a core of neutral lipids surrounded by a phospholipid monolayer with bound proteins. Much of the information on lipid droplet function comes from proteomic and lipodomic studies that identify the components of droplets isolated from organisms throughout the phylogenetic tree. Here, we add to that important inventory by reporting lipid droplet factors from the fission yeast, *Schizosaccharomyces pombe*. Unique to this study was the fact that cells were cultured in three different environments: 1) late log growth phase in glucose-based media, 2) stationary phase in glucose-based media, and 3) late log growth phase in media containing oleic acid. We confirmed colocalization of major factors with lipid droplets using live-cell fluorescent microscopy. We also analyzed droplets from each of the three conditions for sterol ester (SE) and triacylglycerol (TAG) content, along with their respective fatty acid compositions. We identified a previously undiscovered lipid droplet protein, Vip1p, which affects droplet size distribution. The results provide further insight into the workings of these ubiquitous organelles.

Introduction

Lipid droplets are energy storage organelles (Martin and Parton, 2006; Farese and Walther, 2009; Guo *et al.*, 2009; Murphy *et al.*, 2009; Walther and Farese, 2009, 2012; Beller *et al.*, 2010; Fujimoto and Parton, 2011; Ohsaki *et al.*, 2014; Pol *et al.*, 2014). Structurally, they consist of a phospholipid monolayer - with bound and embedded proteins - that surrounds a hydrophobic core of neutral lipids. It is widely accepted that lipid droplets form from the endoplasmic reticulum (ER) when the local concentration of neutral lipids in the cytosolic side of the ER bilayer exceeds a threshold causing the budding of a nascent droplet (Ploegh, 2007; Farese and Walther, 2009; Ohsaki *et al.*, 2009; Walther and Farese, 2009; Pol *et al.*, 2014). After formation, droplet behavior is less clear. This is partially due to the complexity of their relationships with other organelles including the ER (Leber *et al.*, 1998; Wu *et al.*, 2000; Martin and Parton, 2006; Fei *et al.*, 2009; Ohsaki *et al.*, 2009; Hartman *et al.*, 2010; Jacquier *et al.*, 2011, 2013; Kassan *et al.*, 2013), peroxisomes (Binns *et al.*, 2006; Zehmer *et al.*, 2009), mitochondria (Pu *et al.*, 2011), endosomes (Liu *et al.*, 2007), and vacuoles (Gaspar *et al.*, 2008; Van Zutphen *et al.*, 2014). However, proteomic studies on isolated droplets have uncovered many factors that potentially modulate droplet interactions with these organelles and have been crucial for determining droplet behavior (Leber *et al.*, 1994; Wu *et al.*, 2000; Milla *et al.*, 2002; Brasaemle *et al.*, 2004; Fujimoto *et al.*, 2004; Jolivet *et al.*, 2004; Liu *et al.*, 2004; Umlauf *et al.*, 2004; Connerth *et al.*, 2009; Low *et al.*, 2010; Grillitsch *et al.*, 2011; Zhang *et al.*, 2011, 2012; Du *et al.*, 2013; Ivashov *et al.*, 2013; Krahmer *et al.*, 2013; Schmidt *et al.*, 2014). Even with such an impressive inventory of lipid droplet-associated proteins from a wide-range of organisms, gaps in our knowledge still exist. Here we aim to help fill this void by studying the protein and neutral lipid compositions of lipid droplets isolated from the fission yeast, *Schizosaccharomyces pombe*.

We determined the protein and neutral lipid content of lipid droplets isolated from fission yeast *S. pombe* cells that were split into three categories: 1) cells in late log growth phase grown in glucose-rich media, 2) cells in stationary phase grown in glucose-rich media, and 3) cells in late log growth phase grown in media supplemented with 0.1% oleic acid. Many of the factors matched those identified in previous proteomic studies of lipid droplet proteins isolated from other organisms, especially budding yeast (Leber *et al.*, 1994; Athenstaedt *et al.*, 1999; Binns *et al.*, 2006; Wolinski and Kohlwein, 2008; Connerth *et al.*, 2009; Grillitsch *et al.*, 2011; Ivashov *et al.*, 2013; Currie *et al.*, 2014; Schmidt *et al.*, 2014). We identified a novel lipid droplet protein, Vip1p, which localizes strongly to lipid droplets in fission yeast cells. Cells lacking this factor have abnormally large droplet sizes.

Materials and Methods

Fission yeast strains

We used protease-deficient *S. pombe* TM011 cells as the starting point for our experiments (Sirotkin *et al.*, 2005). All yeast strains were constructed using the techniques of Bahler *et al.* (1998). Strains expressing fluorescent fusion proteins were constructed as follows. Long C-terminal-binding primers were designed using the Bahler website. These primers were used in PCR reactions with pKS390 from Snaith *et al.* (2005) as the template. Fission yeast cells were transformed with the PCR products using a standard lithium acetate protocol. Cells were selected for kanMX6 and integrations were confirmed by diagnostic PCR. The *vip1Δ* strain was created by similar techniques. Long N-terminal primers were designed using the Bahler website. These primers were used in PCR reactions with JQ1 from Bahler *et al.* (1998) as the template. The

transformation and diagnostic PCR protocols were identical to those for the fluorescent fusion protein constructs.

Yeast cell culture

Set 1 cells were grown to late log phase to an optical density (O.D.) of ~0.8 at 30°C in yeast extract plus five supplement (YE5S) media (Sunrise Science Products, #2011). Set 2 cells were grown to stationary phase to an OD of ~19 at 30°C in YE5S. Set 3 cells were grown to an OD of 0.4 at 30°C in YE5S. The cells were then pelleted in a Sorvell Legend XTR centrifuge for 5 min at 3,800 × *g*. The YE5S was removed and the cells were resuspended in YPO (0.5% yeast extract, 0.1% oleic acid, 0.2% Tween 80, 0.1% glucose, 0.5% peptone, and 0.3% potassium phosphate) and incubated at 30°C for an additional four h at which point their OD reached ~0.8.

Lipid droplet isolation

We followed the exact protocol described in detail in Ref. Mannik *et al.* (2014) for the isolation of lipid droplets from *S. pombe* cells using density gradient centrifugation as the central technique. We confirmed the purity of the lipid droplet floating layer using Western blot analysis. Antibodies to Erg7p (dilution 1:5000), Cpy1p (dilution 1:5000), and Pma1p (dilution 1:10,000) were a gift from Gunter Daum (Graz). Antibodies to Dpm1p (4 μg/ml) were purchased from Abcam. Secondary antibodies were IRDye 680 goat anti-rabbit (dilution 1:15,000) or IR dye 800 CW goat anti-mouse IgG (dilution 1:5,000).

Protein extraction

We added diethyl ether to the lipid droplet fraction in a 3:2 volume:volume ratio and vortexed the combined sample every 5 min over 20 min total at 25°C. The diethyl ether separated the

proteins from the lipid droplets with the proteins remaining in the aqueous phase. We then centrifuged the mixture in 1.5 ml tubes at 25°C for 10 min at 17,000 × *g* in a Fisher Scientific AccuSpin Micro 17 centrifuge. The upper phase containing the diethyl ether was removed and discarded. Residual diethyl ether remaining on the top of the aqueous layer was removed by evaporation under a steady stream of N2 at 25°C. 100% trichloroacetic acid (TCA) was added to the aqueous phase at 4°C for 1 h to ensure a final concentration of 10% TCA in order to precipitate the proteins. Samples were then spun at 4°C for 20 min at 17,000 × *g* and any remaining TCA was removed, followed by a wash with chilled acetone. Any residual acetone was removed and the protein pellet was stored in at -80°C.

Digestion of proteins

Proteins extracted from the lipid droplet fraction were solubilized in guanidine buffer [6 M Guanidine HCl, 10 mM DTT in Tris buffer (100 mM Tris; 10 mM CaCl2), pH 7.6], and incubated at 60°C for 4 h. Following incubation, a 25 µl sample was used for protein estimation and the rest of the sample was diluted 6-fold using Tris buffer (100 mM Tris; 10 mM CaCl2, pH 7.6) amended with trypsin (Promega) and subjected to overnight proteolysis at 37°C with gentle mixing as described before (Thompson *et al.*, 2007). Following trypsin digestion, the peptides were amended with 10 mM DTT, and incubated at 37°C for 1 h. The reaction was stopped by adding 10% formic acid to a final concentration of 0.1% and the peptide samples were stored at -80°C until mass spectrometry analysis. All chemicals were obtained from Sigma Chemical Co., unless specified otherwise. High performance liquid chromatography- (HPLC-) grade water, acetonitrile and acetone were obtained from Burdick & Jackson and 99% formic acid was purchased from EM Science. Total protein present in a sample was estimated using the RC/DC

protein estimation kit (Bio-Rad Laboratories) per the manufacturer's protocol using protein standard (supplied in the kit) for the assay.

2D-LC-MS/MS analysis

A single aliquot of peptide mix (~70 µg) was pressure loaded onto an in-house SCX (Luna, Phenomenex)-C18 (Aqua, Phenomenex) resin packed column as previously described [Brown *et al.*, 2006; Thompson *et al.*, 2007]. The sample column was desalted offline [Chourey *et al.*, 2013] then connected to a C18 packed PicoFrit tip (New Objective) interfaced with an LTQ Orbitrap instrument (Thermo Scientific). The peptides were chromatographically separated and analyzed via 24 h Multi-Dimensional Protein Identification Technology (Mu-DPIT) approach as previously described (Thompson *et al.*, 2007; Sharma *et al.*, 2012) using three salt pulses (30, 60, and 100% of 500 mM ammonium acetate followed by 120 min elution gradient). Peptide fragmentation data were collected using LTQ-Orbitrap, operated in data-dependent mode and under the control of Xcalibur software (Thermo Scientific). LTQ Orbitrap was set to 30K resolution while the rest of the settings were maintained as previously described (Sharma *et al.*, 2012). Each of the three protein sets was run in triplicate. The MS/MS data obtained was searched against *Schizosaccharomyces pombe* 972 h genome using the SEQUEST algorithm (Eng *et al.*, 1994). A list of commonly occurring contaminants was concatenated to the database for identification and removal of the mentioned proteins from the final data. The resultant datasets were sorted using DTASelect (Tabb *et al.*, 2002) under set parameters: fully tryptic peptides only with ΔCN of at least 0.08 and cross-correlation scores (Xcorr) of at least 1.8 (+1), 2.5 (+2), 3.5 (+3) and identification of at least two peptides per protein sequence was a prerequisite for protein identifications. Spectral counts of identified peptides were normalized as

described before (Paoletti *et al.*, 2006) and the normalized spectral abundance factor (NSAF) was used as a relative measure of protein abundance.

Neutral lipid extraction and analysis

Neutral lipids were extracted from previously purified lipid droplets using 2 volumes of chloroform:methanol (1:3). Samples were vortexed for 1 min followed by centrifugation at 1,000 × *g* for 10 min at 25°C. The lower organic phase was isolated and dried under a stream of N_2 at 25°C and resuspended in 100 µl of chloroform. Samples were then separated on TLC plates (Whatman Diamond LK6F Silica Gel 60 Å, 4500) using hexane:diethyl ether:acetic acid (70:30:1), Commercially available cholesteryl oleate (Sigma-Aldrich, C9253) and glyceryl trioleate (Sigma-Aldrich, T7140) were used as standards. Phospholipids were extracted using similar methods. TLC was performed using a different solvent system consisting of chloroform:methanol:water (65:25:4). For samples separated via TLC and ultimately quantified by GC-MS, bands were identified using UV light instead of iodine and scraped off the TLC plates. Lipids were removed from the silica using a 1:1 chloroform:methanol mixture, followed by sonication, which was then repeated. Samples were dried overnight and resuspended in 100 µl of methanol.

For GC-MS, dried samples were resuspended in 100 µl of methanol followed by the addition of 300 µl 2% H_2SO_4 in methanol. Esterification was completed by a 4 h incubation at 80°C with mixing every 30 min. 300 µl of 0.9% NaCl was added, along with 300 µl of hexane, containing 5 mg/L pentadecanoic acid. Samples were vortexed, spun for 3,000 × *g* for 3 min, and stored at -20°C until further analysis.

The GC-MS run was conducted using the HP6890 GC-MS system equipped with a HP 5973 mass selective detector and a 30 m × 0.25 mm i.d., 0.25 μm film thickness DB5 column (Phenomenex Inc.) with an attached 10 m guard column. A 1 μl portion of the extracted sample was injected into the DB5 column using splitless injection (1 μl at 280°C). Helium was used as a carrier gas (1.1 μl /min). The mass transfer line and ion source were set at 250°C and 200°C, respectively. Esters were detected with electron ionization in both scan mode (50 to 450 m/z) and selected ion monitoring mode for each compound (for quantitative analysis). The column temperature was initially held at 160°C for 1 min, then increased by 20°C per min for 7 min until 300°C. Products were detected using the following SIM parameters: ions 74.00, 87.00, 143.00, and 256.00 C12 from 3.50–4.50 min, ions 74.00, 87.00, and 242.00 detected from 4.50–5.20 min for C14, ions 74.10 detected from 5.20–5.65 min for C15, ions 74.00, 87.00, and 143 detected from 5.65–6.50 min for C16 and 16:1, ions 74.00, 88.00, and 312.00 detected from 6.50-tfinal min for C18 and C18:1.

Live cell fluorescent microscopy

We reserved 20 ml each of the three sets of cells to determine the distribution and number of lipid droplets. Cells were pelleted at 25°C for 5 min at 3,800 × *g* in a swinging bucket centrifuge. The supernatants were removed and the cells were resuspended in 1 ml of fresh YE5S and transferred to new 1.5 ml tubes. Cells from Set 3 were washed three times with 1 ml of YE5S to remove any oleic acid, which interferes with BODIPY 493/503 staining of neutral lipids. 1 ml of cells was then transferred to new 1.5 ml tubes that contained 10 μl of a 100 μM stock of BODIPY 493/503 in ethanol. Thus the final concentration of BODIPY 493/503 was 1 μM (Long *et al.*, 2012). All three samples were pelleted at 25°C for 10 min at 1,000 × *g* in a Fisher Scientific AccuSpin Micro 17 centrifuge and the supernatant was removed down to 100 μl. The

cells were resuspended and 2 µl aliquots were placed between a glass cover slip (Fisher Scientific; #12-542-B) and a microscope slide (Fisher Scientific; #12-544-7). Images were collected on a Leica SP2 laser scanning confocal microscope and an EVOS inverted microscope equipped with a 100x objective (Advanced Microscopy Group). Fission yeast strains expressing fluorescent fusion proteins from native loci were created using the techniques of Bahler *et al.* (1998). BODIPY 493/503 was added to the cells in the exact manner as above and the cells were subsequently imaged as above.

Results

We performed three sets of experiments to determine the protein and neutral lipid composition of lipid droplets isolated from fission yeast *S. pombe* cells that were 1) mitotic (Fig. 1A), 2) post-mitotic (Fig. 1B), 3) mitotic and incubated in media supplemented with free fatty acids (Fig. 1C). We grew the first set of cells to late log phase in glucose-rich media (Set 1), the second set of cells to stationary phase in glucose-rich media (Set 2), and the third set of cells in glucose-rich media, after which, the cells were pelleted and resuspended in media containing 0.1% oleic acid (YPO) for an additional 4 h of incubation until they reached late log phase (Set 3). In the first experiment, we aimed to determine factors responsible for neutral lipid storage during cell growth; in the second experiment, we aimed to determine factors responsible for neutral lipid storage in post-mitotic eukaryotes; and in the third experiment, we aimed to determine factors responsible for neutral lipid storage when eukaryotic cells were dividing in the presence of high levels of freely diffusing fatty acids (oleic acid). The number of BODIPY 493/503-stained cellular lipid droplets increased in cells from Set 1 to cells in both Set 2 and Set 3 by a factor of two (Fig. 1D).

Lipid droplet associated proteins

We obtained droplets from the three sets of cells using the recently published lipid droplet isolation protocol based on density gradient centrifugation (Mannik *et al.*, 2014). The enrichment of lipid droplets and the depletion of other organelles in the floating layer after each centrifugation step was confirmed by Western blot analysis as performed in Mannik *et al.* (2014). In brief, Erg7p (lipid droplet marker [Milla *et al.*, 2002]) became enriched in the floating layer while Pma1p (plasma membrane marker [Binns *et al.*, 2006]) and Cpy1p (vacuole marker) became completely depleted (Fig. 2). Dpm1p (ER marker [Binns *et al.*, 2006; Takeda and Nakano, 2008; Grillitsch *et al.*, 2011; Ayciriex *et al.*, 2012]) was significantly depleted in the lipid droplet floating layer as seen previously (Binns *et al.*, 2006; Grillitsch *et al.*, 2011).

We identified the differences in the proteins bound to the isolated lipid droplets using mass spectrometry. Factors were sorted in decreasing order by their average adjusted NSAF scores across the three sets: raw spectral counts were normalized by NSAF and then multiplied by 100,000 from two independent runs of each sample. The 25 most abundant proteins from each condition, along with their predicted functionalities, are listed in Tables 1–3. The delta-sterol C-methyltransferase, Erg6p and squalene monooxygenase, Erg1p, were among the highest in all three, which is in agreement with previous work (Ayciriex *et al.*, 2012). An RNA-binding protein, Vip1p, had significant populations in all three conditions. To our knowledge Vip1p has not previously been associated with lipid droplets. To ensure the colocalization of Erg6p, Erg1p, and Vip1p to lipid droplets, we created individual strains expressing Erg6p-mCherry, Erg1p-mCherry, and Vip1p-mCherry from their native loci. We grew each of these strains expressing fluorescent fusion proteins in the described conditions for all three sets, stained lipid droplets with BODIPY 493/503, and performed Epi fluorescence microscopy experiments to determine

the extent of colocalization. Erg6p-mCherry and Erg1p-mCherry localized strongly to BODIPY 493/503-stained lipid droplets in all three sets (Fig. 3A–F). Vip1p-mCherry colocalized with BODIPY 493/503 in all three conditions, although a diffuse, cytosolic signal was still present (Fig. 3G–I).

Other than Erg1p, Erg6p, and Vip1p, several other proteins were present in multiple conditions, which are listed in bold in Tables 1–3, and many of which have been seen in previous lipid droplet proteomic studies in other organisms (Binns *et al.*, 2006; Fei *et al.*, 2011; Grillitsch *et al.*, 2011; Ayciriex *et al.*, 2012; Currie *et al.*, 2014). Our other notable findings included, Lcf1p, an acyl-CoA ligase; Rer2p, a predicted cis-prenyltransferase; SPAC3A11.10c, a dipeptidyl peptidase, and Env9p; a short chain dehydrogenase. Ribosomal peptides were also detected throughout, and Sets 2 and 3 contained higher incidences of mitochondrial proteins.

We created a *vip1Δ* strain (Fig. 4A), which we cultured in our three growth and feeding conditions. Differences were seen in droplet morphologies between *vip1Δ* and wild-type cells that were both grown to stationary phase in YE5S. Droplets in *vip1Δ* cells were "super-sized" compared to those in wild-type cells (Fig. 4B and C). Droplet sizes in *vip1Δ* and wild-type cells were statistically equivalent in sets 1 and 3 (not shown). It is not clear why this is the case. Vip1p has a predicted RNA recognition motif from Asn-3 to Gly-76, however, lipid binding domains were not evident using prediction software. (Fig. 4D). This factor does not appear to have a mammalian ortholog.

Lipid droplet neutral lipids

We extracted neutral lipids from isolated lipid droplets using the techniques of Ref. Hsieh *et al.* (2012). Thin layer chromatography (TLC) was used to confirm sterol esters (SEs) and

triacylglycerols (TAGs) as the primary components of *S. pombe* lipid droplets (Fig. 5). The neutral lipid compositions of the isolated lipid droplets from the three sets as measured by image analysis of the TLC bands and represented in ratios of SE:TAG were 58:42 (Set 1), 45:55 (Set 2), and 45:55 (Set 3). Additional bands representing fatty acids and sterols were also present, but these were relatively minor and not ultimately quantified. We used GC-MS to analyzed whole lipid droplet fractions and detected sizable peaks for the following fatty acids: laurate (12:0), myristate (14:0), palmitate (16:0), palmitoleate (16:1), stearate (18:0), and oleate (18:1). In order to quantify specific neutral lipid fatty acids, species were again separated via iodine-free TLC, as this covalently modifies fatty acids data (data not shown).

As expected, the neutral lipid profiles of the isolated droplets varied slightly between sets (Table 4). The neutral lipid compositions of the isolated lipid droplets from the three sets as measured by GC-MS and represented in ratios of SE:TAG were 56:44 (Set 1), 36:64 (Set 2), and 47:53 (Set 3). We also determined the fatty acid composition of the two major neutral lipid classes. Unlike budding yeast, SEs in *S. pombe* are primarily saturated (Table 5). In all three sets palmitate (16:0) and stearate (18:0) were routinely the dominant species. SEs isolated from purified lipid droplets from cells in stationary phase were slightly more enriched with oleate resulting in decreased saturation. TAG species had consistently more unsaturated fatty acids than their SE counterpart (Table 6), and it has been proposed that the higher fluidity of TAG over SEs may drive droplet formation (Ayciriex *et al.*, 2012). TAG from Set 2 droplets contained noticeable differences as nearly half of its acyl groups were C18:1 which compensated for its loss in C16. Interestingly in the presence of oleic acid (18:1), TAG species contained less C18:1.

Discussion

We determined the protein and neutral lipid composition of lipid droplets isolated from fission yeast *S. pombe* cells as a function of cell growth phase and the free fatty acid content of the media in which the cells were cultured. We performed three sets of experiments where droplets were isolated from fission yeast cells grown to 1) late log phase in glucose rich media, 2) stationary phase in glucose rich media, and 3) late log phase in the presence of oleic acid. We presented the top twenty factors in each set based on their normalized NSAF scores. Approximately 30% of our total identified factors have been previously identified in the lipid droplet fraction of lipid droplet proteomic studies (Athenstaedt *et al.*, 1999; Beller *et al.*, 2006; Binns *et al.*, 2006; Fei *et al.*, 2011; Grillitsch *et al.*, 2011; Zhang *et al.*, 2011; Ayciriex *et al.*, 2012; Ding *et al.*, 2012; Du *et al.*, 2013; Krahmer *et al.*, 2013; Currie *et al.*, 2014).

Because of similarly high Vip1p abundances within all three sets, we expected Vip1p to possess a major role in droplet function. Upon *vip1* deletion, cells appeared phenotypically normal during mitotic conditions. We saw the biggest difference in *vip1*Δ cell droplets during instances of increased neutral lipid sequestration, as droplets in these cells were fewer in number but larger than those in wild-type cells. It is unclear how Vip1p localizes to lipid droplets as it lacks a sequence that may be buried in the membrane. Other RNAbinding proteins have been identified in previous droplet proteomes, however their levels were not nearly as high as other established lipid droplet factors and thus thought to be artifacts. Mechanistically, Vip1p function remains unclear, though it could be translationally regulating other enzymes affecting droplet formation and or growth.

We also identified several proteins that have recently been implicated to affect lipid droplet dynamics. The *S. cerevisiae* ortholog of the short chain dehydrogenase, Env9p, was recently shown to localize to droplets and facilitate expansion (Siddiqah *et al.*, 2015). Env9p reductase

activity was found to be directed at HMG-CoA, a rate limiting step within the sterol synthesis pathway. Elevated levels of the cis-prenyltransferase, Rer2p, were also present in Sets 1 and 2. This factor was recently found to localize with droplets in a high-confidence study (Currie *et al.*, 2014). An *rer2* knockout induced a 2-fold increase of SEs in budding yeast (Currie *et al.*, 2014). The discovery of SPAC3A11.10c, which functions as dipeptidyl peptidase, was an interesting result as it lacks a budding yeast ortholog. Expression of its human ortholog, DPPIV, induces both adipocyte differentiation and lipid accumulation and is an active target studied for the treatment of type-2 diabetes (Rosmaninho-Salgado *et al.*, 2012; Aroor *et al.*, 2015).

Also of great interest to droplet formation and subsequent growth are the relative contributions of the lipid metabolizing enzymes. In this study, the fatty acid-CoA ligase, Lcf1p, was found at its highest abundance in Set 1. The human ortholog of Lcf1p, acyl-CoA synthetase 3 (GI:4758330), has been found to promote lipid droplet biogenesis in COS-1 cells (Kassan *et al.*, 2013) and the acyl-CoA synthetase 4 isoenzymes mediate the metabolic flux of fatty acids towards phosphatidylinositol (Kuch *et al.*, 2014).

Factors that initiate neutral lipid breakdown are typically found in the lipid droplet fraction. Their colocalization with lipid droplets has been widely documented using fluorescent fusion proteins with much focus on the *tgl* family of gene products (Kurat *et al.*, 2009), which in *S. pombe* include the TAG lipases Ptl1p, Ptl2p, and Ptl3p. All three factors were detected in each set with Ptl2p having the highest signal. Ayr1p may be an additional contributor to TAG lipolysis, which is normally required for the biosynthesis of LPA via the acylation of 1-acyl-DHAP, but has recently been identified as a triacylglycerol lipase in *S. cerevisiae* (Ploier *et al.*, 2013). These lipases hydrolyze fatty acids from TAG and transform them into usable chemical energy via β-oxidation. In higher eukaryotes, this process takes place in mitochondria, however

in yeast it is generally considered to occur in peroxisomes. In contrast to budding yeast and the methylotropic yeast *Pichia pastoris* whose lipid droplets contained strong peroxisomal relationships (Binns *et al.*, 2006; Ivashov *et al.*, 2013), here we encountered negligible peroxisomal factors. This, coupled with the increase of mitochondrial factors in Sets 2 and 3, suggests *S. pombe* may rely heavily on mitochondria for β-oxidation. Peroxisome biogenesis has been observed in fission yeast cells after 20 h of incubation in oleic acid-based media (Jourdain *et al.*, 2008), but only at levels 2.5 times less than in *S. cerevisiae*, suggesting alternative methods for fatty acid metabolism in *S. pombe.*

The discovery of ribosomal and protein synthesis factors of the cyclophilin family peptidyl-prolyl cis-trans isomerase Cyp4p (*cyp4*) in the lipid droplet fraction lends weight to the theory that protein synthesis may occur close to or on the surfaces of lipid droplets potentially as they remain in contact with the ER (Jacquier *et al.*, 2011). The synthesis and translocation of lipid droplet proteins from the ribosome has long been puzzling because of the need for these factors to be incorporated into the unique monolayer geometry of the lipid droplet. Cyclophilin B regulates the distribution of ApoB-100 on cellular lipid droplets, and cyclophilin A is essential for hepatitis C virus replication, both in hepatocytes (Kaul *etal.*, 2009). Hepatitis C replication has been directly linked to aspects of lipid droplet formation (Boulant *et al.*, 2008; Herker *et al.*, 2010; Lyn *et al.*, 2010). Thus, genetic studies on the *cyp4* gene in yeast may provide insight into lipid droplet protein translocation and lipid droplet formation mechanisms. Both the targeting of proteins to lipid droplets and the dissociation of proteins from lipid droplets have been areas of intense interest and will mostly likely involve a variety of mechanisms including translocation of factors from the ER (Wilfling *et al.*, 2013) and potentially from other organelles such as ribosomes and the Golgi.

Acknowledgements

This work was supported by American Heart Association award 13SDG14500046 to P.D. The authors thank Dr. Gunther Daum (Technische Universitat Graz) for antibodies for Western blots, Eric T. Boder (Univ. of Tennessee) for the use of his shaking incubators, tabletop centrifuge, and Western blot analysis equipment; Donovan Layton and Cong Trinh for the use of their GC-MS; and the Center for Environmental Biotechnology (Univ. of Tennessee) for the use of their ultracentrifuge. K.C. and R.L.H. acknowledge the financial support provided by the U.S. Department of Energy, Office of Biological and Environmental Research, Genome Sciences Program. Oak Ridge National Laboratory is managed by the University of Tennessee, Battelle LLC for the Department of Energy.

References

Aroor, A.R., Habibi, J., Ford, D.A., Nistala, R., Lastra, G., Manrique, C., Dunham, M.M., Ford, K.D., Thyfault, J.P., Parks, E.J., *et al.*2015. Dipeptidyl peptidase-4 inhibition ameliorates Western dietnduced hepatic steatosis and insulin resistance through hepatic lipid remodeling and modulation of hepatic mitochondrial function. *Diabetes* 64, 1988–2001.

Athenstaedt, K., Zweytick, D., Jandrositz, A., Kohlwein, S.D., and Daum, G. 1999. Identification and characterization of major lipid particle proteins of the yeast *Saccharomyces cerevisiae*. *J. Bacteriol.* 181, 6441–6448.

Ayciriex, S., Le Guédard, M., Camougrand, N., Velours, G., Schoene, M., Leone, S., Wattelet-Boyer, V., Dupuy, J.W., Shevchenko, A., Schmitter, J.M., *et al.* 2012. *YPR139c/LOA1* encodes a novel lysophosphatidic acid acyltransferase associate with lipid droplets and involved in TAG homeostasis. *Mol. Biol. Cell.* 23, 233–245.

Bahler, J., Wu, J.Q., Longtine, M.S., Shah, N.G., McKenzie, A., Steever, A.B., Wach, A., Philippsen, P., and Pringle, J.R. 1998. Heterologous modules for efficient and versatile PCR-based gene targeting in *Schizosaccharomyces pombe*. *Yeast* 14, 943–951.

Beller, M., Riedel, D., Jänsch, L., Dieterich, G., Wehland, J., Jäckle, H., and Kühnlein, R.P. 2006. Characterization of the drosophila lipid droplet subproteome. *Mol. Cell Proteomics* 5, 1082–1094.

Beller, M., Thiel, K., Thul, P.J., and Jackle, H. 2010. Lipid droplets: a dynamic organelle moves into focus. *FEBS Lett.* 584, 2176–2182.

Binns, D., Januszewski, T., Chen, Y., Hill, J., Markin, V.S., Zhao, Y., Gilpin, C., Chapman, K.D., Anderson, R.G., and Goodman, J.M. 2006. An intimate collaboration between peroxisomes and lipid bodies. *J. Cell Biol.* 173, 719–731.

Boulant, S., Douglas, M.W., Moody, L., Budkowska, A., Target-Adams, P., and McLauchlan, J. 2008. Hepatitis C virus core protein induces lipid droplet redistribution in a microtubule- and dynein-dependent manner. *Traffic* 9, 1268–1282.

Brasaemle, D.L., Dolios, G., Shapiro, L., and Wang, R. 2004. Proteomic analysis of proteins associated with lipid droplets of basal and lipolytically stimulated 3T3-L1 adipocytes. *J. Biol. Chem.* 279, 46835–46842.

Brown, S.D., Thompson, M.R., VerBerkmoes, N.C., Chourey, K., Shah, M., Zhou, J., Hettich, R.L., and Thompson, D.K. 2006. Molecular dynamics of the *Shewanella oneidensis* respinse to chromate stress. *Mol. Cell Proteomics* 5, 1054–1071.

Chourey, K., NIssen, S., Vishnivetskava, T., Shah, M., Pfiffner, S., Hettich, R.L., and Löffler, F.E. 2013. Environmental proteomics reveals early microbial community responses to biostimulation at a uranium- and nitrate-contaminated site. *Proteomics* 13, 2912–2930.

Connerth, M., Grillitsch, K., Köfeler, H., and Daum, G. 2009. Analysis of lipid particles from yeast. *Methods Mol Biol.* 579, 359–374.

Currie, E., Gou, X., Christiano, R., Chitraju, C., Kory, N., Harrison, K., Haas, J., Walther, T.C., and Farese, R.V.Jr. 2014. High confidence proteomic analysis of yeast LDs identifies additional droplet proteins and reveals connections to dolichol synthesis and sterol acetylation. *J. Lipid Res.* 55, 1465–1477.

Ding, Y., Wu, Y., Zeng, R., and Liao, K. 2012. Proteomic profiling of lipid droplet-associated proteins in primary adipocytes of normal and obese mouse. *Acta Biochim. Biophys. Sin (Shanghai).* 44, 394–406.

Du, X., Barisch, C., Paschke, P., Herrfurth, C., Bertinetti, O., Pawolleck, N., Otto, H., Rühling, H., Feussner, I., Herberg, F.W., *et al.* 2013. *Dictyostelium* lipid droplets host novel proteins. *Eukaryot. Cell* 12, 1517–1529.

Eng, J.K., McCormack, A.L., and Yates, J.R. 1994. An approach to correlate tandem mass spectral data of peptides with amino acid sequences in a protein database. *J. Am. Soc. Mass Spectrom.* 5, 976–989.

Farese, R.V.Jr. and Walther, T.C. 2009. Lipid droplets finally get a little R-E-S-P-E-C-T. *Cell* 139, 855–860.

Fei, W., Wang, H., Fu, X., Bielby, C., and Yang, H. 2009. Conditions of endoplasmic reticulum stress stimulate lipid droplet formation in *Saccharomyces cerevisiae*. *Biochem. J.* 424, 61–67.

Fei, W., Zhong, L., Ta, M.T., Shui, G., Wenk, M.R., and Yang, H. 2011. The size and phospholipid composition of lipid droplets can influence their proteome. *Biochem. Biophys. Res. Commun.* 415, 455–462.

Fujimoto, Y., Itabe, H., Sakai, J., Makita, M., Noda, J., Mori, M., Higashi, Y., Kojima, S., and Takano, T. 2004. Identification of major proteins in the lipid droplet-enriched fraction isolated from the human hepatocyte cell line HuH7. *Biochim. Biophys. Acta* 1644, 47–59.

Fujimoto, T. and Parton, R.G. 2011. Not just fat: the structure and function of the lipid droplet. *Cold Spring Harb. Perspect. Biol.* 3, a004838.

Gaspar, M.L., Jesch, S.A., Viswanatha, R., Antosh, A.L., Brown, W.J., Kohlwein, S.D., and Henry, S.A. 2008. A block in endoplasmic reticulum-to-golgi trafficking inhibits phospholipid synthesis and induces neutral lipid accumulation. *J. Biol. Chem.* 283, 25735–25751.

Grillitsch, K., Connerth, M., Köfeler, H., Arrey, T.N., Rietschel, B., Wagner, B., Karas, M., and Daum, G. 2011. Lipid particles/droplets of the yeast *Saccharomyces cerevisiae* revisited: lipidome meets proteome. *Biochim. Biophys. Acta* 1811, 1165–1176.

Guo, Y., Cordes, K.R., Farese, R.V.Jr., and Walther, T.C. 2009. Lipid droplets at a glance. *J. Cell Sci.* 122, 749–752.

Hartman, I.Z., Liu, P., Zehmer, J.K., Luby-Phelps, K., Jo, Y., Anderson, R.G., and DeBose-Boyd, R.A. 2010. Sterol-induced dislocation of 3-hyroxy-3-methylglutaryl coenzyme A reductase from endoplasmic reticulum membranes into the cytosol through a subcellular compartment resembling lipid droplets. *J. Biol. Chem.* 285, 19288–19298.

Herker, E., Harris, C., Hernandez, C., Carpentier, A., Kaehlcke, K., Rosenberg, A.R., Farese, R.V.Jr., and Ott, M. 2010. Efficient hepatitis C virus particle formation requires diacylglycerol acyltransferase-1. *Nat. Med.* 16, 1295–1298.

Hsieh, K., Lee, Y.K., Londos, C., Raaka, B.M., Dalen, K.T., and Kimmel, A.R. 2012. Perilipin family members preferentially sequester to either triacylglycerol-specific or cholesteryl-ester-specific intracellular lipid storage droplets. *J. Cell Sci.* 125, 4067–4076.

Ivashov, V.A., Grillitsch, K., Koefeler, H., Leitner, E., Baeumlisberger, D., Kara, M., and Daum, G. 2013. Lipidome and proteome of lipid droplets from the methylotrophic yeast *Pichia pastoris*. *Biochim. Biophys. Acta* 1831, 282–290.

Jacquier, N., Choudhary, V., Mari, M., Toulmay, A., Reggiori, F., and Schneiter, R. 2011. Lipid droplets are functionally connected to the endoplasmic reticulum in *Saccharomyces cerevisiae*. *J. Cell Sci.* 124, 2424–2437.

Jacquier, N., Mishra, S., Choudhary, V., and Schneiter, R. 2013. Expression of oleosin and perilipins in yeast promotes formation of lipid droplets from the endoplasmic reticulum. *J. Cell Sci.* 126, 5198–5209.

Jolivet, P., Roux, E., D'Andrea, S., Davanture, M., Negroni, L., Zivy, M., and Chardot, T. 2004. Protein composition of oil bodies in *Arabidopsis thaliana* ecotype WS. *Plant Physiol Biochem.* 42, 501–509.

Jourdain, I., Sontam, D., Johnson, C., Dillies, C., and Hyams, J.S. 2008. Dynamin-dependent biogenesis, cell cycle regulation and mitochondrial association of peroxisomes in fission yeast. *Traffic* 9, 353–365.

Kassan, A., Herms, A., Fernández-Vidal, A., Bosch, M., Schieber, N.L., Reddy, B.J., Fajardo, A., Gelabert-Baldrich, M., Tebar, F., Enrich, C., *et al*. 2013. Acyl-CoA synthetase 3 promotes lipid droplet biogenesis in ER microdomains. *J. Cell Biol.* 203, 985–1001.

Kaul, A., Stauffer, S., Berger, C., Pertel, T., Schmitt, J., Kallis, S., Zayas, M., Lohmann, V., Luban, J., and Bartenschlager, R. 2009. Essential role of cyclophilin A for hepatitis C virus replication and virus production and possible link to polyprotein cleavage kinetics. *PLoS Pathog.* 5, e1000546.

Krahmer, N., Hilger, M., Kory, N., Wilfling, F., Stoehr, G., Mann, M., Farese, R.V.Jr., and Walther, T.C. 2013. Protein correlation profiles identify lipid droplet proteins with high confidence. *Mol. Cell. Proteomics* 12, 1115–1126.

Küch, E.M., Vellaramkalayil, R., Zhang, I., Lehnen, D., Brugger, B., Sreemmel, W., Ehehalt, R., Poppelreuther, M., and Füllekrug, J. 2014. Differentially localized acyl-CoA synthetase 4 isoenzymes mediate the metabolic channeling of fatty acids towards phosphatidylinositol. *Biochim. Biophys. Acta* 1841, 227–239.

Kurat, C.F., Wolinski, H., Petschnigg, J., Kaluarachchi, S., Andrews, B., Natter, K., and Kohlwein, S.D. 2009. Cdk1/Cdc28-dependent activation of the major triacylglycerol lipase Tgl4 in yeast links lipolysis to cell-cycle progression. *Mol. Cell* 33, 53–63.

Leber, R., Zinser, E., Zellnig, G., Paltauf, F., and Daum, G. 1994. Characterization of lipid particles of the yeast, *Saccharomyces cerevisiae*. *Yeast* 10, 1421–1428.

Leber, R., Landl, K., Zinser, E., Ahorn, H., Spok, A., Kohlwein, S.D., Turnowsky, F., and Daum, G. 1998. Dual localization of squalene epoxidase, Erg1p, in yeast reflects a relationship between the endoplasmic reticulum and lipid particles. *Mol. Biol. Cell* 9, 375–386.

Liu, P.S., Bartz, R., Zehmer, J.K., Ying, Y.S., Zhu, M., Serrero, G., and Anderson, R.G.W. 2007. Rab-regulated interaction of early endosomes with lipid droplets. *Biochim. Biophys. Acta* 1773, 784–793.

Liu, P., Ying, Y., Zhao, Y., Mundy, D.I., Zhu, M., and Anderson, R.G. 2004. Chinese hamster ovary K2 cell lipid droplets appear to be metabolic organelles involved in membrane traffic. *J. Biol. Chem.* 279, 3787–3792.

Long, A.P., Manneschmidt, A.K., VerBrugge, B., Dortch, M.R., Minkin, S.C., Prater, K.E., Biggerstaff, J.P., Dunlap J.R., and Dalhaimer, P. 2012. Lipid droplet *de novo* formation and fission and cell cycle dependent in fission yeast. *Traffic* 13, 705–713.

Low, K.L., Shui, G., Natter, K., Yeo, W.K., Kohlwein, S.D., Dick, T., Rao, S.P., and Wenk, M.R. 2010. Lipid droplet-associated proteins are involved in the biosynthesis and hydrolysis of triacylglycerol in *Mycobacterium bovis* bacillus calmette-guerin. *J. Biol. Chem.* 285, 21662–21670.

Lyn, R.K., Kennedy, D.C., Stolow, A., Ridsdale, A., and Pezacki, J.P. 2010. Dynamics of lipid droplets induced by the hepatitis C virus core protein. *Biochem. Biophys. Res. Commun.* 399, 518–524.

Mannik, J., Meyers, A., and Dalhaimer, P. 2014. Isolation of cellular lipid droplets: two purification techniques starting from yeast cells and human placentas. *J. Vis. Exp.* 86, e50981.

Martin, S. and Parton, R.G. 2006. Lipid droplets: a unified view of a dynamic organelle. *Nat. Rev. Mol. Cell Biol.* 9, 367–377.

Milla, P., Athenstaedt, K., Viola, F., Oliaro-Bosso, S., Kohlwein, S.D., Daum, G., and Balliano, G. 2002. Yeast oxidosqualene cyclase (Erg7p) is a major component of lipid particles. *J. Biol. Chem.* 277, 2406–2412.

Murphy, S., Martin, S., and Parton, R.G. 2009. Lipid droplet-organelle interactions; sharing the fats. *Biochim. Biophys. Acta* 1791, 441–447.

Ohsaki, Y., Cheng, J., Suzuki, M., Shinohara, Y., Fujita, A., and Fujimoto, T. 2009. Biogenesis of cytoplasmic lipid droplets: from the lipid ester globule in the membrane to the visible structure. *Biochim. Biophys. Acta* 1791, 399–407.

Ohsaki, Y., Suzuki, M., and Fujimoto, T. 2014. Open questions in lipid droplet biology. *Chem. Biol.* 21, 86–96.

Paoletti, A.C., Parmely, T.J., Tomomori-Sato, C., Sato, S., Zhu, D.X., Conaway, R.C., Conaway, J.W., Florens, L., and Washburn, M.P. 2006. Quantitative proteomic analysis of distinct mammalian mediator complexes using normalized spectral abundance factors. *Proc. Natl. Acad. Sci. USA* 103, 18928–18933.

Ploegh, H.L. 2007. A lipid-based model for the creation of an escape hatch from the endoplasmic reticulum. *Nature* 448, 435–438.

Ploier, B., Scharwey, M., Kock, B., Schmidt, C., Schatte, J., Rechberger, G., Kollroser, M., Hermetter, A., and Daum, G. 2013. Screening for hydrolytic enzymes reveals ayr1p as a novel triacylglycerol lipase in *Saccharomyces cerevisiae*. *J. Biol. Chem.* 288, 36061–36072.

Pol, A., Gross, S.P., and Parton, R.G. 2014. Biogenesis of the multifunctional lipid droplet: lipids, proteins, and sites. *J. Cell Biol.* 3, 635–646.

Pu, J., Ha, C.W., Zhang, S.Y., Jung, J.P., Huh, W.K., and Liu, P. 2011. Interactomic study on interaction between lipid droplets and mitochondria. *Protein Cell* 2, 487–496.

Rosmaninho-Salgado, J., Marques, A.P., Estrada, M., Santana, M., Cortez, V., Grouzmann, E., and Cavadas, C. 2012. Dipeptidylpeptidase- IV by cleaving neuropeptide Y induces lipid accumulation and PPAR-γ expression. *Peptides* 37, 49–54.

Schmidt, C., Ploier, B., Koch, B., and Daum, G. 2014. Analysis of yeast lipid droplet proteome and lipidome. *Methods Cell Biol.* 116, 15–37.

Sharma, R., Dill, B.D., Chourey, K., Shah, M., VerBerkmoes, N.C., and Hettich, R.L. 2012. Coupling a detergent lysis/cleanup methodology with intact protein fractionation for enhanced proteome characterization. *J. Proteome Res.* 11, 6008–6018.

Siddiqah, I., Manandhar, S., and Gharakhanian, E. 2015. Yeast Env9 is a conserved oxidoreductase involved in lipid droplet biogenesis. *FASEB J.* 29, 574.10.

Sirotkin, V., Beltzner, C.C., Marchand, J.B., and Pollard, T.D. 2005. Interactions of WASp, myosin-I, and verprolin with Arp2/3 complex during actin patch assembly in fission yeast. *J. Cell Biol.* 170, 637–648.

Snaith, H.A., Samejima, I., and Sawin, K.E. 2005. Multistep and multimode cortical anchoring of tea1p at cell tips in fission yeast. *EMBO J.* 24, 3690–3699.

Tabb, D.L., McDonald, W.H., and Yates, J.R. 2002. DTASelect and contrast: tools for assembling and comparing protein identifications from shotgun proteomics. *J. Proteome Res.* 1, 21–26.

Takeda, Y. and Nakano, A. 2008. *In vitro* formation of a novel type of membrane vesicles containing Dpm1p, putative transport vesicles for lipid droplets in budding yeast. *J. Biochem.* 143, 803–811.

Thompson, M.R., VerBerkmoes, N.C., Chourey, K., Shah, M., Thompson, D.K., and Hettich, R.L. 2007. Dosage-dependent proteome response of *Shewanella oneidensis* MR-1 to acute chromate challenge. *J. Proteome Res.* 6, 1745–1757.

Umlauf, E., Csaszar, E., Moertelmaier, M., Schuetz, G.J., Parton, R.G., and Prohaska, R. 2004. Association of stomatin with lipid bodies. *J. Biol. Chem.* 279, 23699–23709.

Van Zutphen, T., Todde, V., de Boer, R., Kreim, M., Hofbauer, H.F., Wolinski, H., Veehuis, M., van der Klei, I.J., and Kohlwein, S.D. 2014. Lipid droplet autophagy in the yeast *Saccharomyces cerevisiae*. *Mol. Biol. Cell.* 25, 290–301.

Walther, T.C. and Farese, R.V.Jr. 2009. The life of lipid droplets. *Biochim. Biophys. Acta.* 1791, 459–466.

Walther, T.C. and Farese, R.V.Jr. 2012. Lipid droplets and cellular lipid metabolism. *Annu. Rev. Biochem.* 81, 687–714.

Wilfling, F., Wang, H., Haas, J.T., Krahmer, N., Gould, T.J., Uchida, A., Cheng, J.X., Graham, M., Christiano, R., Fröhlich, F., *et al.* 2013. Triacylgylcerol synthesis enzymes mediate lipid droplet growth by relocalizing from the ER to lipid droplets. *Dev. Cell* 24, 384–399.

Wolinski, H. and Kohlwein, S.D. 2008. Microscopic analysis of lipid droplet metabolism and dynamics in yeast. *Methods Mol. Biol.* 457, 151–163.

Wu, C.C., Howell, K.E., Neville, M.C., Yates, J.R., and McManaman, J.L. 2000. Proteomics reveal a link between the endoplasmic reticulum and lipid secretory mechanisms in mammary epithelial cells. *Electrophoresis* 21, 3470–3482.

Zehmer, J.K., Huang, Y.G., Peng, G., Pu, J., Anderson, R.G.W., and Liu, P.S. 2009. A role for lipid droplets in inter-membrane lipid traffic. *Proteomics* 9, 914–921.

Zhang, P., Na, H., Liu, Z., Zhang, S., Xue, P., Chen, Y., Pu, J., Peng, G., Huang, X., Yang, F., *et al.* 2012. Proteomic study and marker protein identification of caenorhabditis elegans lipid droplets. *Mol. Cell. Proteomics* 11, 317–328.

Zhang, H., Wang, Y., Li, J., Yu, J., Pu, J., Li, L., Zhang, H., Zhang, S., Peng, G., Yang, F., *et al*. 2011. Proteome of skeletal muscle lipid droplet reveals association with mitochondria and apolipoprotein A-I. *J. Proteome Res.* 10, 4757–4768.

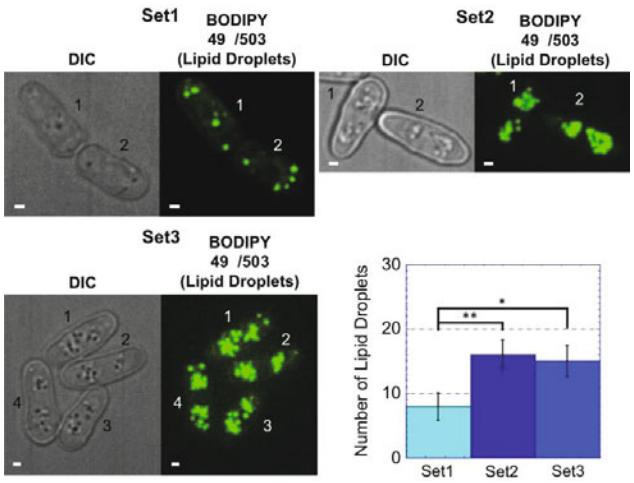

Figure 1. The number of lipid droplets varies in fission yeast cells based on the growth phase and the amount of free fatty acids in the media. (A-C) DIC images (left panels) and maximum intensity projections of all z-stacks from confocal microscopy experiments (right panels) of fission yeast cells where the lipid droplets have been stained with BODIPY 493/503 (green). Intensities of the green channels are increased in the images to aid the viewer in seeing small droplets. (A) Set 1 cells grown to late log phase in glucose-based media, (B) Set 2 cells grown to stationary phase in glucose-based media, and (C) Set 3 cells grown in glucose-based media and then pelleted and grown to late log phase in the presence of 0.1% oleic acid. Cells are labeled by number for ease of visualization. (D) Plot of the number of lipid droplets per cell in fifty cells from each of the three sets. Error bars are the standard deviation. * $P < 0.0001$; ** $P < 0.0001$. Scale bars are 1 micron.

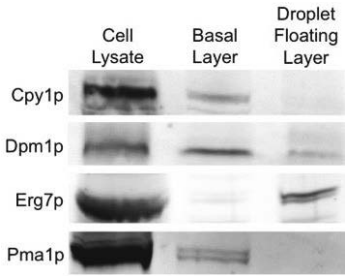

Figure 2. Western blots of the fractions from the lipid droplet isolation protocol. Antibodies for specific organelle markers Cpy1p (vacuole), Dpm1p (ER), Erg7p (lipid droplets), and Pma1p (plasma membrane) were incubated with unique fractions from the lipid droplet isolation in determine purity of the lipid droplet floating layer.

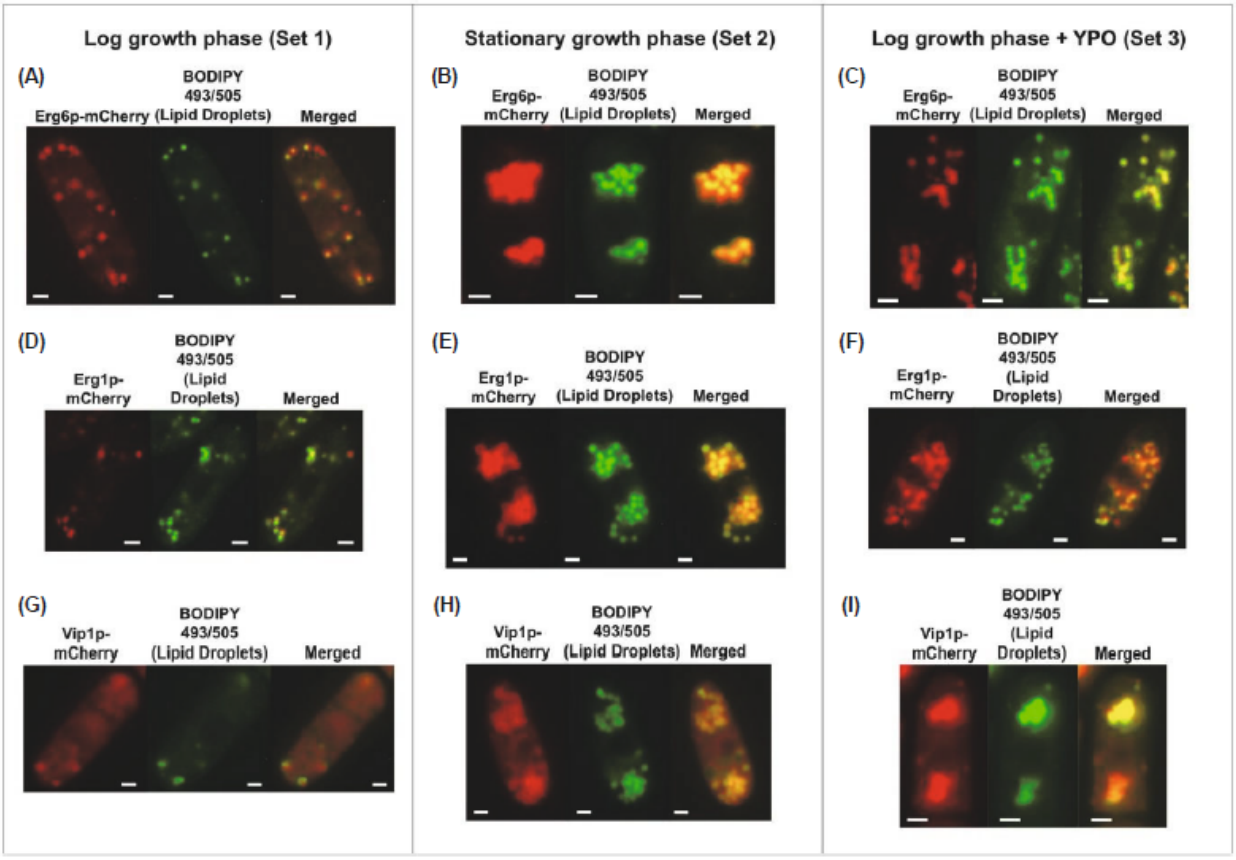

Figure 3. Cellular localization of the factors with the highest NSAF scores across all three sets of experiments. (A-I) Single-plane fluorescent micrographs of fission yeast cells expressing the indicated fluorescent fusion protein from the native locus (left panel) where the lipid droplets were stained with the neutral lipid dye BODIPY 493/503 (center panel), and the merger of the two signals (right panel). Intensities of the green channels are increased in the images to aid the viewer in seeing small droplets. (A-C) Vip1p-mCherry, (D-F) Erg1p-mCherry, and (G-I) Erg6p-mCherry. Scale bars are 1 micron.

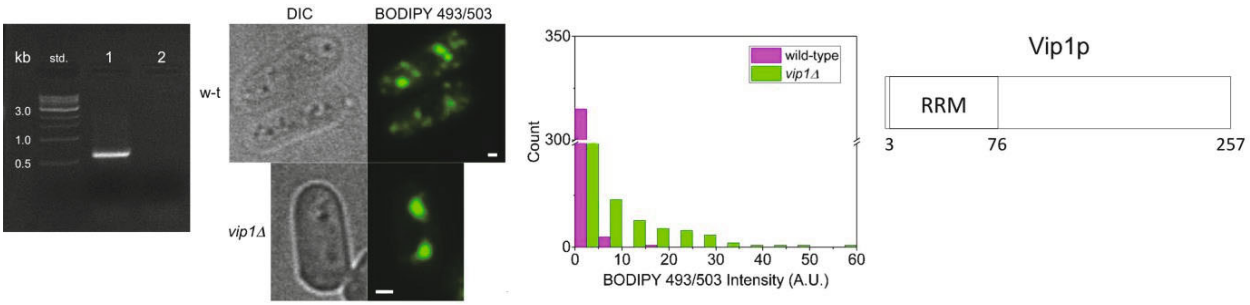

Figure 4. *vip1Δ* cells showed increased lipid droplet sizes compared to droplets in wild-type cells. (A) DNA gel showing the diagnostic PCR product of cells lacking *vip1* (lane 1) versus wild-type cells (lane 2). (B) DIC and maximum intensity confocal microscopy images of wild-type and *vip1Δ* cells that were grown to stationary phase and stained with BODIPY 493/503. Scale bars are one micron. (C) Plot of the distribution of lipid droplet fluorescent intensity in thirty wild-type cells and thirty *vip1Δ* cells. There is a break in the vertical axis between counts of 50 and 300. (D) Schematic diagram of *S. pombe* Vip1p with the predicted RNA recognition motif (RRM).

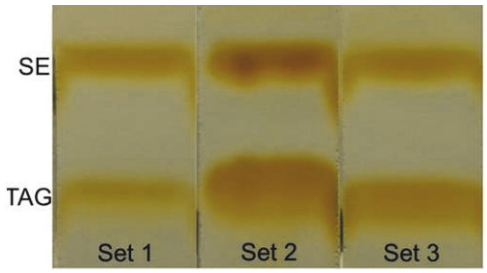

Figure 5. Neutral lipid composition of lipid droplets isolated from *S. pombe* cells. (A-C) Images of thin layer chromatography results for (A) Set 1, (B) Set 2, and (C) Set 3.

Table 1. Top 25 factors identified in Set 1.

Gene	Predicted function	Score
Erg6	delta-sterol C-methyltransferase	51.5280
Vip1	RNA-binding protein	47.4815
Erg1	Squalene monooxygenase	7.2082
SPAC18G6.12c	Hypothetical protein	6.8060
Lcf1	long-chain-fatty-acid-CoA ligase	6.0194
Cyp4	Cyclophilin family peptidyl-prolyl cis-trans isomerase	4.3134
Pgk1	Phosphoglycerate kinase	4.0888
Tdh1	glyceraldehyde-3-phosphate dehydrogenase	3.8497
Env9	Short chain dehydrogenase	3.7265
Kar2	BiP	3.4309
Hsp10	Mitochondrial heat shock protein	3.3644
Eno101	enolase	3.3123
Tif38	Translation initiation factor eIF3h (p40)	2.9589
Pgc1	Glycerophosphoryl diester phosphodiesterase	2.7987
Vma2	V-type ATPase V1 subunit B	2.2860
Eif6	Translation initiation factor eIF3f	2.1928
Rer2	cis-prenyltransferase	2.0257
Rps1601	40S ribosomal protein S16	2.0205
HIs2	Histidinol dehydrogenase	2.0001
Rpl35	60S ribosomal protein L35	1.9563
Lys3	Saccharopine dehydrogenase	1.8896
Rpl302	60S ribosomal protein L36	1.8825
Pyk1	Pyruvate kinase (predicted)	1.8090
Ef1-a	Translational elongation factor EF-1alpha	1.7455
Ef1-c	Translational elongation factor EF-1alpha	1.7455

Table 2. Top 25 factors identified in Set 2.

Gene	Predicted function	Score
Erg1	Squalene monooxygenase	13.7965
Erg6	delta-sterol C-methyltransferase	13.1150
Tef101	Translation elongation factor EF-1 alpha Ef1a-a	5.5494
Tef103	Translation elongation factor EF-1 alpha Ef1a-c	5.5494
Tef103	Translation elongation factor EF-1 alpha Ef1a-b	4.4313
SPAC3A11.10c	Dipeptidyl peptidase	4.3654
Kar2	BiP	3.9947
Hsp10	Mitochondrial heat shock protein Hsp10	3.5504
Env9	Short chain dehydrogenase	3.2413
Ilv5	Acetohydroxyacid reductoisomerase	3.0079
Rpl3601	60S ribosomal protein L36	2.7148
Hsp60	Mitochondrial heat shock protein	2.6860
Rho1	Rho family GTPase Rho1	2.6517
Htb1	Histone H2B alpha Htb1	2.5763
Atp2	F1-ATPase beta subunit Atp2	2.4634
Rer2	cis-prenyltransferase	2.4234
Vip1	RNA-binding protein Vip1	2.3283
Erg26	3 beta-hydroxysteroid dehydrogenase/delta5→4-isomerase	2.2299
Mdh1	Malate dehydrogenase	2.1430
Rpl402	60S ribosomal protein L2	2.0886
Cox4	Cytochrome c oxidase subunit IV (predicted)	2.0617
Tdh1	Glyceraldehyde-3-phosphate dehydrogenase	2.0496
Rps17	40S ribosomal protein S17	2.0330
SPAC4D7.02c	Glycerophosphoryl diester phosphodiesterase (predicted)	1.8657
	60S Ribosomal protein 20	1.8598

Table 3. Top 25 factors identified in Set 3.

Gene	Predicted function	Score
Vip1	RNA-binding protein	13.7427
Hsp10	Mitochondrial heat shock protein	7.4196
Ilv5	Acetohydroxyacid reductoisomerase	5.2188
Erg6	delta-sterol C-methyltransferase	4.1876
Hsp60	Mitochondrial heat shock protein	4.0952
Mdh1	Malate dehydrogenase	3.4702
Tef101	Translation elongation factor EF-1 alpha Ef1a-a	3.3670
Tef103	Translation elongation factor EF-1 alpha Ef1a-c	3.3670
Tef102	Translation elongation factor EF-1 alpha Ef1a-b	3.3670
Por1	Mitochondrial outer membrane voltage-dependent anion-selective channel	3.2418
Hsp70	Mitochondrial heat shock protein	3.1263
Anc1	Mitochondrial adenine nucleotide carrier	3.0706
SPBC16A3.02c	Mitochondrial peptidase	3.0074
Pgc1	Glycerophosphoryl diester phosphodiesterase	2.9798
Atp7	F0-ATPase subunit D	2.8885
Atp2	F1-ATPase beta subunit	2.7455
SPAC3A11.10c	Dipeptidyl peptidase	2.6146
Kar2	BiP	2.4638
Env9	Short chain dehydrogenase	2.4402
Ayr1	1-acyldihydroxyacetone phosphate reductase	2.2465
Erg1	Squalene monooxygenase (predicted)	2.0856
Atp4	F0-ATPase subunit	2.0800
Atp1	F1-ATPase alpha subunit	1.8612
Qcr7	Ubiquinol-cytochrome-c reductase complex subunit 6	1.8430
Qcr2	Ubiquinol-cytochrome-c reductase complex core protein Qcr2	1.8244

Table 4. Lipid droplet neutral lipid quantification from GC-MS.

	Total Mass %	
	TAG	SE
Set 1	44.3	55.7
Set 2	63.7	36.3
Set 3	53.1	46.9

Table 5. Fatty acid analysis of sterol esters from Sets 1-3.

	SE by Mass %							
	C12	C14	C16:1	C16	C18:1	C18	% Unsaturated	% Saturated
Set 1	3.4	1.9	4.3	39.2	11.9	39.3	16.2	83.8
Set 2	3.2	1.7	3.2	34.0	19.3	38.6	22.5	77.5
Set 3	2.9	2.0	3.8	40.3	8.7	42.3	12.5	87.5

Table 6. Fatty acid analysis of triacylglycerols from Sets 1-3.

	TAG by Mass %							
	C12	C14	C16:1	C16	C18:1	C18	% Unsaturated	% Saturated
Set 1	2.4	1.4	2.7	30.5	28.0	35.0	30.7	69.3
Set 2	2.3	0.9	2.1	17.2	46.2	31.4	48.3	51.7
Set 3	1.3	3.2	5.7	30.4	18.2	41.1	23.9	76.1